Production of Titanium Deposits by Cold-Gas Dynamic Spray: Numerical Modeling and Experimental Characterization

T. Marrocco, D.G. McCartney, P.H. Shipway, and A.J. Sturgeon

Over the past five years, interest in cold-gas dynamic spraying (CGDS) has increased substantially. Considerable effort has been devoted to process development and optimization for such metals as copper and aluminium. This paper describes work undertaken to expand the understanding of the deposition of titanium by cold-spray methods. CGDS deposits have been produced from commercially pure titanium using room-temperature helium gas. The effect of different powder particle size ranges, types of substrate, substrate preparation methods, and spray parameter conditions on powder deposition have been investigated. Microhardness testing of deposits was conducted, and their microstructures have been examined by scanning electron microscopy. Samples for pull-off bond-strength tests have been prepared from a number of the more promising sets of spray parameters and adhesive strengths determined. A one-dimensional numerical model of particle acceleration, employing isentropic gas flow behavior in the nozzle, has also been used to estimate particle exit velocities. This model explicitly addresses the dependence of the drag coefficient on gas compressibility and demonstrates its significance in terms of predicted particle velocities. By linking this model with the measured particle size distributions, estimates of particle velocity distributions at the nozzle exit plane have been computed. These allow an approximate value of the critical velocity for deposition of titanium to be made. Experimental observations on the microstructure and properties of the deposits are discussed in light of powder particle size and velocity distributions and the underlying physical and mechanical properties of the powders and substrates.

Keywords	cold-gas dynamic spray, microstructure, numerical modeling, properties, titanium

1. Introduction

Cold-gas dynamic spray (CGDS) is a coating technology in which powder particles in the solid state are accelerated by a supersonic gas jet to impact with a substrate to form a thick (~100 μm to 1 mm) deposit. The principles of powder particle acceleration arising from gas flow through a de Laval-type converging/diverging nozzle are summarized elsewhere (Ref 1, 2). Deposit initiation and build-up occur via plastic deformation of particles on impact at high velocity (300-1200 m s^{-1}) and at a temperature generally well below the melting point of the feedstock powder. It has been reported that a wide range of metallic materials, e.g., copper, aluminum, nickel, tin, and zinc, can be deposited by cold spraying onto a variety of metallic and nonmetallic substrates (Ref 3-8). It is generally accepted that the

T. Marrocco, D.G. McCartney, and **P.H. Shipway,** School of Mechanical, Materials and Manufacturing Engineering, University of Nottingham, University Park, Nottingham, NG7 2RD, United Kingdom; **A.J. Sturgeon,** TWI, Granta Park, Great Abington, Cambridge, CB1 6AL, United Kingdom. Contact e-mail: graham.mccartney@ nottingham.ac.uk.

Nomenclature	
A	cross-section area of nozzle, m^2
A^*	throat area of nozzle, m^2
A_p	surface area of the particle, m^2
Bi	biot number
C_d	drag coefficient
C_g	specific heat of the gas, J kg^{-1} K^{-1}
C_p	specific heat of the particle, J kg^{-1} K^{-1}
d_p	diameter of the particle, m
h	heat-transfer coefficient, W m^{-2} K^{-1}
M	mach number of the gas
M_r	relative Mach number of the particle
m_p	mass of the particle, kg
Nu	Nusselt number
R	gas constant, J kg^{-1} K^{-1}
Re	Reynolds number of the particle
Pr	Prandtl number
T_g	temperature of the gas, K
T_p	temperature of the particle, K
t	time, s
v_g	velocity of the gas, m s^{-1}
v_p	velocity of the particle, m s^{-1}
γ	specific heat ratio of the gas
λ_g	thermal conductivity of the gas, W m^{-1} K^{-1}
λ_p	thermal conductivity of the particle, W m^{-1} K^{-1}
μ_g	dynamic viscosity of the gas, kg m^{-1} s^{-1}
ρ_g	density of the gas, kg m^{-3}
ρ_p	density of the particle, kg m^{-3}

sprayed powder must exhibit some degree of ductility at the high strain rate conditions attained on impact in order that shear deformation and cold welding may occur at the surfaces that come into contact.

A number of studies have suggested that the particle deposition behavior is influenced significantly by the particle velocity prior to impact with the substrate. Particle velocity is a function of the spray process conditions, including gas type, pressure, and temperature, and materials properties, such as particle diameter, density, and morphology (Ref 8-10). For a given material, successful deposition requires a certain minimum particle velocity or "critical velocity," the value of which depends most significantly on the thermomechanical properties of the powder and substrate materials (Ref 10-16); below this critical velocity, impacting particles are generally observed to cause erosion of the substrate. Normally, a feedstock powder will contain a range of particle sizes and consequently a distribution of particle velocities in the plume. Therefore, the deposition efficiency of a given powder generally increases with an increase in gas pressure and/or temperature, i.e., as the particle velocity increases.

Some workers have examined the role of substrate surface topography on the formation of a bond between incoming particles and substrate. Tokarev et al. (Ref 17) have suggested that particles impacting a substrate in cold spraying first activate the substrate by roughening it; only once this has occurred is a coating able to initiate and grow. It has also been reported that, with a greater roughening of the substrate surface (going from polished to grit-blasted), deposition efficiency of metallic powders increases slightly (Ref 16). Vlcek et al. (Ref 18) have examined the impact of a range of powder types onto a range of substrate materials in cold spraying. They explained differences in the ability of particles to deposit in terms of the mechanical properties of the particles and substrate and the specific impulse of the impact. They related bonding primarily to the relative ease of deformation of the substrate and particle, and concluded that if the particle was significantly more deformable than the substrate, then adhesion was not possible.

To date, much of the work on particle impact, bonding, and deposition efficiency in the cold-spray process has been concerned with copper or aluminium feedstock powders; much less attention has been paid to the deposition of other metals, such as titanium. However, Karthikeyan et al. (Ref 7) described the formation of porous titanium coatings with a deposition efficiency >80%.

In the current study, titanium powder was deposited onto titanium-alloy substrates by cold spraying using helium at room temperature as the primary gas. The aim of the work was to examine the effect of powder size range, substrate surface condition, and gas stagnation pressure on the coating-substrate bond strength and coating porosity, microhardness, and microstructure. In addition, a one-dimensional numerical model was used to predict particle conditions at the spray-nozzle exit plane, to assist in identifying reasons for the experimental observations.

2. Experimental Methods

2.1 Materials

Two separate batches of commercially pure titanium powder (minimum purity 99 wt.% Ti) with different particle size distri-

Table 1 Parameters describing the surface profile of the substrates as a function of surface preparation method

Surface preparation	R_a, μm	R_z, μm	R_k, μm
Ground	0.21 ± 0.03	1.57 ± 0.16	0.73 ± 0.06
Polished	0.046 ± 0.002	0.46 ± 0.09	0.101 ± 0.005
Grit blasted	2.66 ± 0.06	17.03 ± 0.39	9.13 ± 0.31

Note: Values are the average of three measurements, with standard error of the mean indicated.

butions, referred to as CTi (for coarse powder) and FTi (for fine powder), were used as feedstocks in this study; both were produced by the hydride-dehydride process and were supplied by Active Metals Ltd. (Sheffield, U.K.). The CTi powder had a nominal particle size range of 5-45 μm, whereas the FTi powder had a nominal size range of 5-25 μm. The Vickers microhardness of the titanium powder was ~1.7 GPa measured with a 0.098 N load. Coatings were deposited onto Ti-6 wt.%Al-4 wt.%V (Ti6Al4V) substrates (45 × 45 × 5 mm) for microstructural analysis and bond-strength testing. The Vickers macrohardness of the Ti6Al4V substrate material in the as-received condition was ~3.0 GPa (measured with a 196 N load). The substrate surfaces were finished in three different ways with the specific aim of investigating the effect of surface finish on the deposition behavior of the powders. The surface preparation of the substrates was as follows: (a) ground with SiC paper; (b) polished to a 1 μm diamond finish; (c) grit-blasted with Al_2O_3. The surface profile parameters after each of the preparation routes were measured by stylus surface profilometry (Talysurf CLI 1000 Profilometer, Leicester, U.K.) and are shown in Table 1. All substrates were cleaned with methyl alcohol prior to spraying.

2.2 Cold-Spraying Process

CGDS was performed at the University of Nottingham with an in-house designed de Laval nozzle with a 100 mm long diverging section and an exit-to-throat area expansion ratio of ~7.6. Using room-temperature helium both as the powder carrier and as the primary accelerating gas, a range of processing conditions was used. The primary gas and the carrier gas were supplied from separate sources, with the carrier gas pressure set to ~1 bar above that of the primary gas. The distance between the nozzle exit and the substrate (the stand-off distance) had been previously optimized to 20 mm, and this was used throughout the program. A high-pressure powder feeder (Praxair 1264HP, Indianapolis, IN) capable of operating at pressures of up to 34 bar was used to feed the powder to the CGDS nozzle. The powder feeder wheel speed was fixed at 2 rpm. By measurement of the mass of powder used during an extended spray run, it was found that this wheel speed resulted in a feed rate of ~(270-300) × 10^{-6} kg s^{-1} for both powder types. The substrates were placed in a holder for spraying, and the CGDS gun was traversed relative to the substrates at a nominal traverse speed of 100 mm s^{-1} to generate the coating. Multiple passes of the gun over a given substrate were used to increase the deposit thickness up to ~900 μm. Experiments were carried out to study the influence of primary gas pressure, powder particle size range, and substrate surface preparation on the final structure of the deposits as well as their mechanical properties.

2.3 Characterization of Powders and Coatings

The size distribution of both the coarse and fine powder feed-stock materials was measured by laser diffractometry (Laser Mastersizer, Malvern Instruments, Malvern, U.K.).

Microstructural examination of powders and coatings was performed using a scanning electron microscope (SEM) operated at 20 kV. Secondary electron (SE) imaging was used to examine the particle morphology. To prepare the powder for SEM analysis, a small amount of material was scattered onto an adhesive carbon disk so that all particle sizes could be observed in their original proportions. To study the porosity and microstructure of coatings, cross sections were taken perpendicular to the coating-substrate interface. These were then mounted in conducting resin, ground, and carefully polished to avoid particle pull-out; the final polish was a colloidal silica suspension in hydrogen peroxide (this final stage removes the smeared layer that is commonly produced in polishing of titanium and thus allows the true porosity to be imaged). They were then examined with SEM using back-scattered electron imaging (BSE). Average porosity levels in coatings were measured by image analysis. From BSE images of polished cross sections, nine fields of view (each 4000 μm^2) were examined at a final magnification of 1000×.

Vickers microhardness measurements of deposits were made using a 0.98 N load and 15 s loading time. Ten regularly spaced Vickers indents were made on the midplane of each coating cross section, allowing values of the mean and the standard error of the mean to be determined.

The bond strength of the deposits was measured by using a pull-off adhesion testing machine from DFD Instruments (Woking, Surrey, U.K.), which is designed to achieve a uniform stress distribution over the area under test. To carry out this procedure, circular disks of coating (diameter = 8.16 mm) were sprayed onto a larger substrate of the material used using a mask. The disks were then glued to a test element with a two-component epoxy resin. To strengthen the effective bond between the adhesive and the test elements, and to reduce the possibility of failure at the adhesive interfaces, the surfaces of the test elements were grit-blasted and the deposits were degreased with methyl alcohol immediately prior to gluing. At least three pull-off tests were performed for each set of deposit conditions examined, and values for the mean bond strength and standard error in the mean were calculated.

3. Experimental Results

Figure 1 shows the SE image of the as-received CTi powder; the size distributions of both powders, as measured by laser diffractometry, are shown as cumulative volume percentage plots in Fig. 2. From Fig. 1, the angular morphology of the titanium powder, as expected for hydride-dehydride processed powders, can be clearly observed. Figure 2 shows that the FTi powder had a sharp cut-off at a lower size limit, which was ~7 μm. There was also ~50 vol.% above the nominal 25 μm upper limit. By contrast, the CTi powder had a lower cut-off limit close to 20 μm, and there was a substantial volume fraction, ~60%, above the nominal 45 μm upper limit. The mass mean particle diameters were 28 and 47 μm for the FTi and CTi powders, respectively, while the d_{50} values for the powders were 24 and 42 μm, respectively.
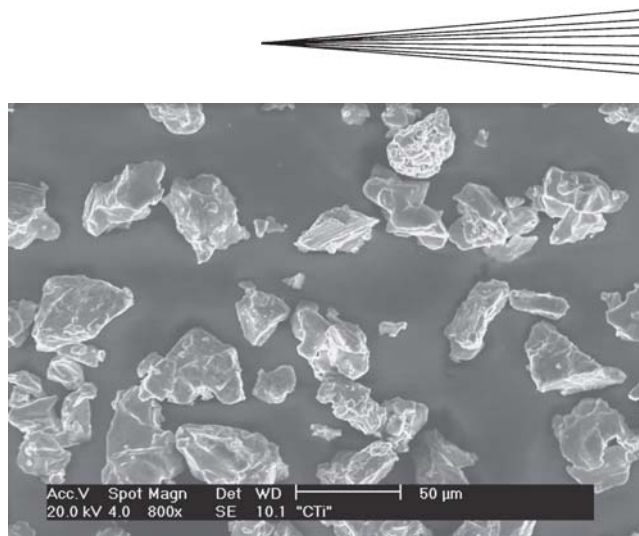
Fig. 1 SE image of a sample of CTi powder showing its morphology
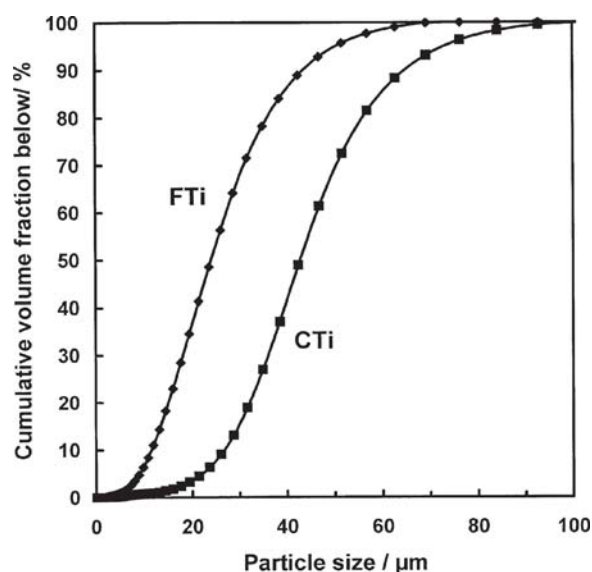

Fig. 2 Cumulative powder size distributions of coarse (CTi) and fine (FTi) titanium powders measured by laser diffractometry

Figure 3 shows BSE-SEM images of the cross sections of the coatings sprayed at 29 bar using the CTi powder (Fig. 3a) and FTi powder (Fig. 3b). The coating deposited from the latter was significantly thicker (almost twice as thick) as that produced from the former under identical conditions but is also seen to exhibit a higher proportion of more regularly distributed porosity. An irregular porous top layer, with a thickness of ~150 μm, is evident in both the coatings, which is probably due to the fact that the last layers to be deposited do not experience such intense peening from non-depositing particles as those that are produced at an earlier stage of deposition.

Figure 4 shows BSE-SEM images of the coating-substrate interface of deposits sprayed onto ground Ti6Al4V using FTi powder at two different gas pressures, namely, 29 bar (Fig. 4a) and 15 bar (Fig. 4b); these were the extreme values of the gas pressures used. These images show that the impact of the incoming titanium particles has not caused significant deformation of
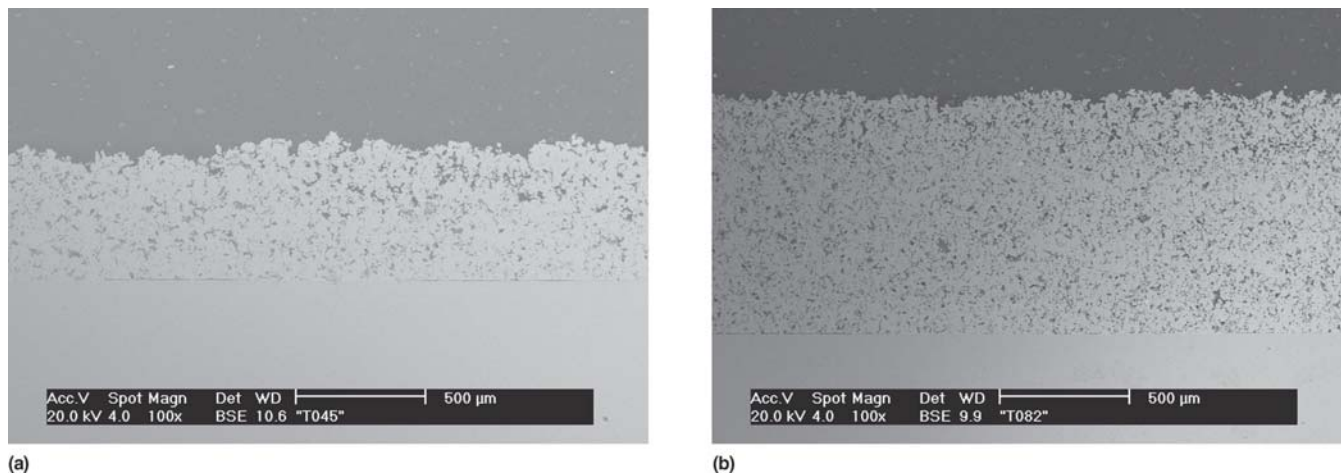
Fig. 3 BSE images of Ti coating cross sections showing different thicknesses and porosity obtained by using (a) coarse and (b) fine Ti powder; both deposits sprayed onto ground Ti6Al4V at 29 bar (thickness: (a) ~530 μm; (b) ~990 μm)
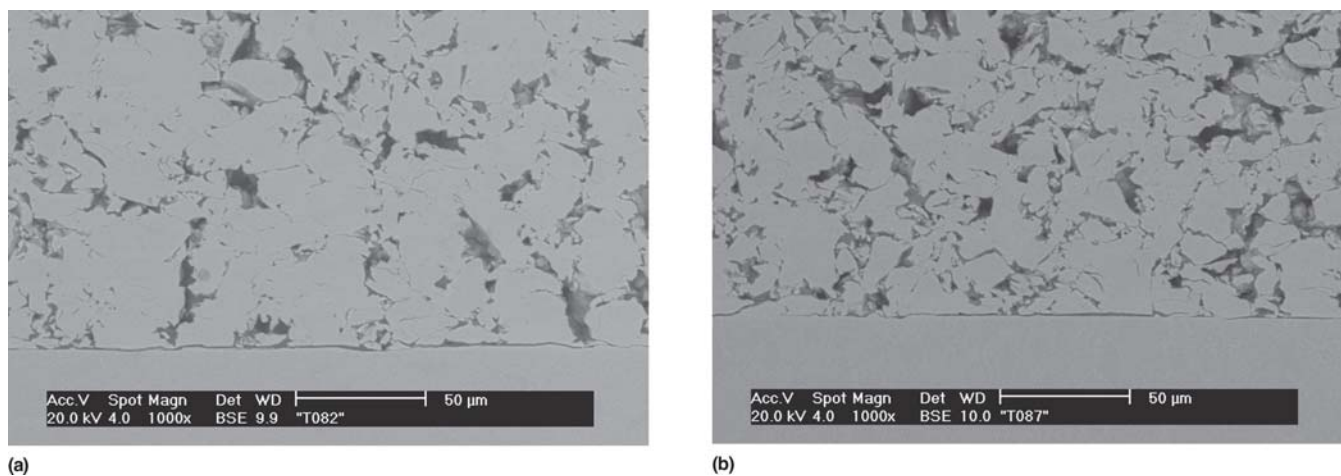

Fig. 4 BSE images of Ti coating cross sections showing different microstructures resulting from spraying FTi powder at different gas pressures: (a) 29 bar and (b) 15 bar (substrate material is Ti6Al4V)

the substrate surface. They also reveal that a significant amount of porosity was present in both deposits. The series of regularly spaced Vickers microhardness indents taken on the cross sections of the coating samples gave a microhardness value for the coatings in a range between 0.88 and 1.77 GPa. In comparison, the hardness of the substrate close to the interface was ~3.34-3.92 GPa, measured with a 0.98 N load.

Micrographs of the deposits formed by spraying the CTi powder at 29 bar onto Ti6Al4V substrates that had been prepared with three different surface conditions are shown in Fig. 5. No significant difference is seen in the profile at the interface in the cases of polished and ground surfaces (Fig. 5a and b). In both cases, the interface is relatively flat and uniform. In contrast, Fig. 5(c) shows an interface with a rougher profile, as expected with grit blasting. The incoming particles appear, at the selected magnification, to have deformed to closely follow the topography of the substrate.

The bond strength between a coating (deposited with CTi

at 29 bar) and substrate, as a function of substrate surface condition, is shown in Fig. 6. It can be seen that the grit-blasted surface condition resulted in the lowest bond strength, with an average strength of ~8 MPa, while the polished and ground surfaces resulted in higher bond strengths of ~22 MPa. Figure 7 shows the bond strength of coatings sprayed with FTi powder onto ground Ti6Al4V substrates as a function of the different primary gas pressures used in the deposition of the coatings. In this case, there was only a small increase in mean bond strength with gas pressure over the range examined. However, magnitudes of the standard error in the mean, particularly at the higher primary gas pressures, are such that no definitive trend can be deduced from the data. Nevertheless, the data do suggest higher variability in deposit adhesion at the higher gas pressures.
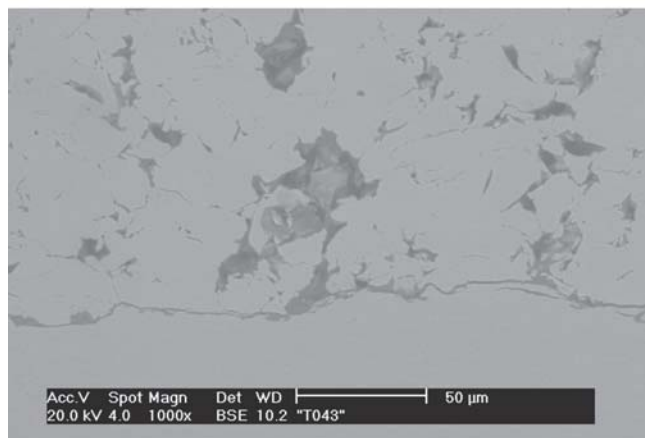
Figure 8 shows the results of image analyses to determine the coating porosity. There is no clear trend in coating porosity with stagnation pressure for coatings deposited with FTi powder onto
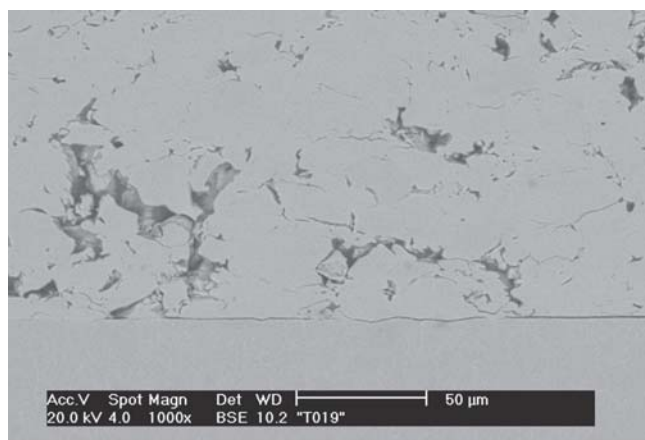
(a)
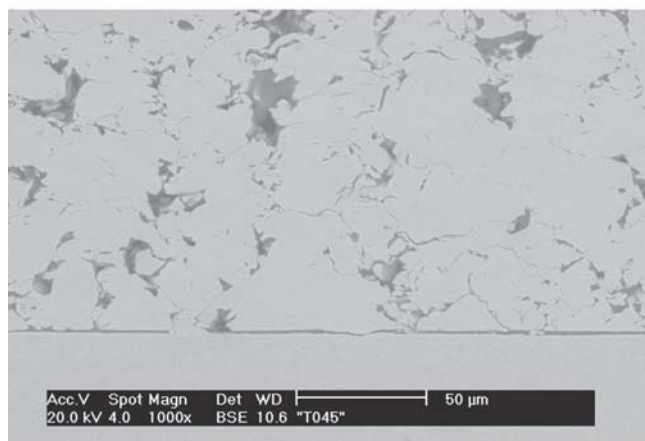
(b)

(c)

Fig. 5 BSE images of Ti coating cross sections deposited from CTi powder onto Ti6Al4V substrates in the following conditions: (a) polished, (b) ground, and (c) grit-blasted, all sprayed at 29 bar gas pressure

Fig. 6 Bar chart showing the effect of substrate condition on the bond strength of deposits sprayed at 29 bar gas pressure using CTi powder (error bars represent the standard error of the mean)

Fig. 7 Bar chart showing the effect of primary gas pressure on the bond strength of deposits sprayed onto ground Ti6Al4V using FTi powder (error bars represent the standard error of the mean)

ground Ti6Al4V substrates; values were in the range 17-24%. However, a coating sprayed onto ground Ti6Al4V at 29 bar using the CTi powder had a lower porosity level than any of the deposits with FTi powder.
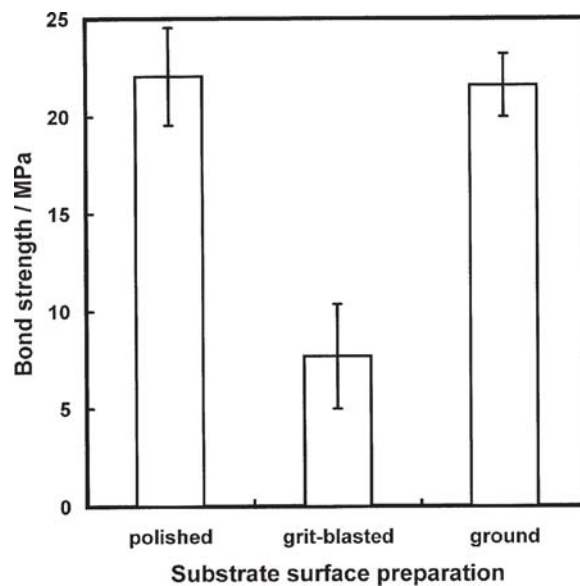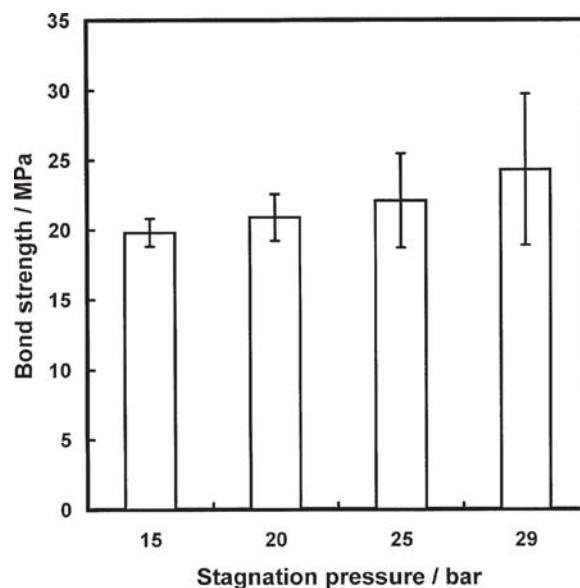
4. Mathematical Model

In recent years, a number of mathematical models of heat and momentum transfer to powder particles in the cold-spray process have been developed (Ref 1, 19-22). Several of them (Ref 1, 19, 20) have been based on one-dimensional isentropic gas flow within the cold-spray nozzle, with powder particles that are accelerated and heated/cooled by interaction with the gas field and that are assumed to travel along the centerline of the nozzle. In
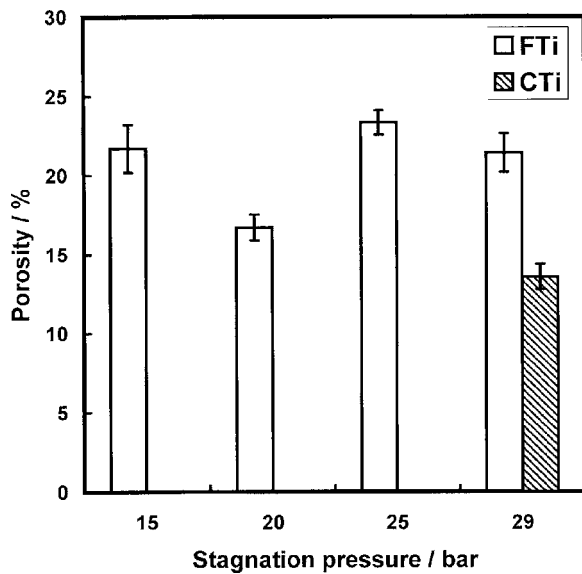
Fig. 8 Porosity of deposits sprayed from FTi and CTi onto ground Ti6Al4V at different gas pressures; values were determined by image analysis, and error bars represent the standard error of the mean

other works (Ref 21, 22), computational fluid dynamics (CFD) analysis has been used to solve the three-dimensional, multi-phase flow problem of powder particle and gas within the nozzle and an Euler-Lagrange approach applied to the coupling between the gas-flow field and the solid particles. However, the published results from both these approaches have largely concentrated on the behavior of copper or aluminium particles in the size range 5-20 μm (Ref 1, 19-22). Thus, a model was specifically developed for the present work so that nozzle exit velocities of titanium powder particles, with diameters up to 80 μm, could be computed to aid the interpretation of the experimental data on deposit build up and observations on coating microstructure formation.

4.1 System Geometry

The model considers a typical converging/diverging nozzle used in cold spray that is axisymmetric with a throat diameter of 2.9 mm, exit diameter of 8.0 mm, and length of 100 mm from the entrance to the exit of the conical diverging section; thus the nozzle expansion ratio is 7.6. Powder particles, assumed to be spherical, are injected with zero initial velocity at the throat and are assumed to travel along the axis of the nozzle. In the cold-spray system used in this work, the powder particles are actually injected into a short convergent section upstream of the throat where the gas flow is subsonic, but this is neglected by the model. Additionally, the model does not consider gas-particle interactions in the region between the nozzle exit and the substrate onto which the powder is deposited.

4.2 Gas-Flow Model

The behavior of the gas along the length of the nozzle is calculated using the assumption of one-dimensional isentropic flow. The governing equations for such behavior, in which flow

is adiabatic and frictionless, are already well established, as detailed elsewhere (Ref 1, 19, 23). In brief, the mathematical relationships that can be derived allow the Mach number, M, of the flow to be determined at different positions along the nozzle from Eq 1 below:

$$\frac{A}{A^*} = \left(\frac{1}{M}\right)\left[\left(\frac{2}{\gamma+1}\right)\left(1+\frac{\gamma-1}{2}M^2\right)\right]^{(\gamma+1)/[2(\gamma-1)]} \tag{Eq 1}$$

In the model, Eq 1 is solved using a standard iterative procedure to obtain values of M for different values of the expansion ratio (A/A^*) corresponding to different positions along the length of the nozzle from throat to exit. Typically, M is determined in steps of 1 mm along the nozzle, which provides a sufficient degree of accuracy for coupling to the particle acceleration and heating model, and then standard relationships (Ref 23) are used to calculate the gas properties, namely, pressure, temperature, density, and velocity, at the same axial locations. In this manner, gas dynamic behavior is computed within the nozzle length, provided no shock waves occur inside it.

4.3 Particle Motion and Heating

The gas properties, as computed above, are then used to calculate the heat and momentum transfer to a particle, assumed to be injected into the gas stream at the throat, as it travels along the nozzle axis. The assumption is also made that the mass flow rate of the particles is sufficiently low so they do not interact with one another, or disturb the gas flow field. This is usually valid for powder flow rates that are ~10-15% of the gas mass flow rate. In the present experimental study, gas mass flow rates were in the range $(10-18) \times 10^{-3}$ kg s^{-1} for the primary gas conditions used, such that powder mass flow rates $[(270-300) \times 10^{-6}$ kg s$^{-1}]$ were significantly less than the critical value that would perturb the gas flows.

The evolution of particle velocity with position is determined using Newton's second law, neglecting all forces acting on the particle other than the drag force due to relative motion between gas and particle. Thus:

$$m_p \frac{dv_p}{dt} = \frac{1}{8} A_p \rho_g C_d |v_g - v_p|(v_g - v_p) \tag{Eq 2}$$

The acceleration for a spherical particle is therefore deduced as:

$$\frac{dv_p}{dt} = \frac{3\rho_g}{4d_p\rho_p} C_d |v_g - v_p|(v_g - v_p) \tag{Eq 3}$$

A number of empirical drag and velocity correlations that are valid when compressibility effects can be neglected have been published in the literature. In the present work, the influence of assumptions about the dependence of C_d on both Reynolds number and Mach number have been explored in some detail. When calculations were performed with the assumption that the drag coefficient depends only on the Reynolds number, the relationships reported by Clift et al. (Ref 24) were used. These are as follows:

$$C_d = \frac{24}{Re} + \frac{3}{16} \qquad (Re < 0.01) \qquad (Eq\ 4a)$$

$$C_d = \frac{24}{Re}(1 + 0.1315Re^{(0.82-0.05w)}) \qquad (0.01 < Re < 20)$$
$$(Eq\ 4b)$$

$$C_d = \frac{24}{Re}(1 + 0.1935Re^{(0.6305)}) \qquad (20 < Re < 260)$$
$$(Eq\ 4c)$$

$$C_d = 1.6435 - 1.1242w + 0.1558w^2 \qquad (260 < Re < 1500)$$
$$(Eq\ 4d)$$

where $w = \log Re$, and the Reynolds number, Re, is defined as follows:

$$Re = \frac{\rho_g |v_g - v_p| d_p}{\mu_g} \qquad (Eq\ 5)$$

However, it is known that the drag coefficient depends not only on Re but also on the Mach number of the flow when compressibility effects are significant, and this has been reported, for example, by Bailey and Hiatt (Ref 25), Walsh (Ref 26), and Henderson (Ref 27). To model this effect, the correlations between C_d, Re, and M proposed by Henderson were introduced in the present work, as was done by Dykhuizen and Smith (Ref 1). These are rather complex, and the reader is referred to Henderson's original paper for details (Ref 27). Briefly, Henderson gives one correlation equation for the subsonic regimen, i.e., $M < 1$, in which C_d is a function of Re and M_r, where M_r is the relative Mach number of the particle in the flow as follows:

$$M_r = \frac{|v_g - v_p|}{\sqrt{\gamma R T_g}} \qquad (Eq\ 6)$$

Henderson also proposes a different correlation relationship for the supersonic regime, when $M > 1.75$ in which C_d depends on both M and Re. In the supersonic region, at values of M between 1 and 1.75, the drag coefficient is determined from a weighted linear interpolation of the C_d values calculated at $M = 1$ and $M = 1.75$.

Physically, the dependence of C_d on M is due to local changes in gas density and shock formation that occur as the particle Mach number exceeds one, thus profoundly affecting the forces acting on it. The graphical representations given by Bailey and Hiatt (Ref 25) reveal that, for Reynolds numbers in the region of 100-1500, the drag coefficient will increase abruptly from ~0.55 to ~1.2 as M increases from ~0.8 to ~1.5, indicating that this could have a significant effect on the particle velocities predicted in the modeling of the cold-spray process.

Heat transfer to a particle is described in the usual manner by a heat-transfer coefficient, h, which is a function of the Nusselt number, Nu. Particles are also assumed to have a uniform temperature at all times, which is a reasonable assumption given that the Biot number of small, high-conductivity particles will be much less than unity. From conservation of energy consider-ations, the equation for temperature change in a particle is thus written as:

$$m_p C_p \frac{dT_p}{dt} = h(T_g - T_p)A_p \qquad (Eq\ 7)$$

where the heat-transfer coefficient, h, is given by:

$$h = \frac{Nu\ \lambda_g}{d_p} \qquad (Eq\ 8)$$

and the Nusselt number, Nu, is obtained from the relationship:

$$Nu = 2 + 0.6Re^{0.5}\ Pr^{1/3} \qquad (Eq\ 9)$$

Combining Eq 8 and 9 and rewriting Eq 7, the rate of change of temperature of a particle is then finally obtained as:

$$\frac{dT_p}{dt} = \frac{6\lambda_g(2 + 0.6Re^{0.5}\ Pr^{1/3})(T_g - T_p)}{d_p^2 \rho_p C_p} \qquad (Eq\ 10)$$

Thus to determine the temperature and velocity of a spherical particle as it moves along the nozzle, Eq 3 and 10 are solved numerically in a series of time steps; typically a time step value of 0.1 μs proved suitable. At the end of each time step, the new velocity, new temperature, and new position of the particle are calculated. Knowing the position of the particle along the nozzle at each time step, the program uses linear interpolation procedures to find the values of gas velocity, pressure, density, and temperature at that location from the isentropic gas-flow field solution. At the beginning of the next time step, these values are then used to update C_d and Nu, recalculate the particle's acceleration and rate of change of temperature, and so determine its new position, temperature, and velocity at the end of the time step. Thus the calculation continues until the particle reaches the exit plane of the nozzle.

Computations were performed for He gas flowing through a converging/diverging nozzle of dimensions given in Section 4.1 at a stagnation pressure of either 15 or 29 bar and stagnation temperature 298 K with titanium particles injected at the throat of the nozzle with zero initial velocity. In this study, the powder particles were not spherical but irregular and angular in shape. This affects their movement in the gas-flow field and consequently their drag coefficients. Irregular particles tend to align themselves with their maximum cross section normal to the flow direction, and their drag coefficients are thus higher than those calculated from an equivalent sphere diameter. However, there is uncertainty over the most appropriate mathematical correlation to use (Ref 28). Therefore, in the present calculations, a simplified analysis using spherical particles of diameter from 1 to 80 μm was used to obtain results relevant to both the coarse and fine powders detailed in Section 2 and to identify trends in behavior. The thermophysical properties assumed for solid titanium and helium gas that were used in the calculations are given in Table 2.

4.4 Model Calculations

The calculated Mach number at the exit plane of the nozzle used in the experimental study, with an expansion ratio of 7.6, is
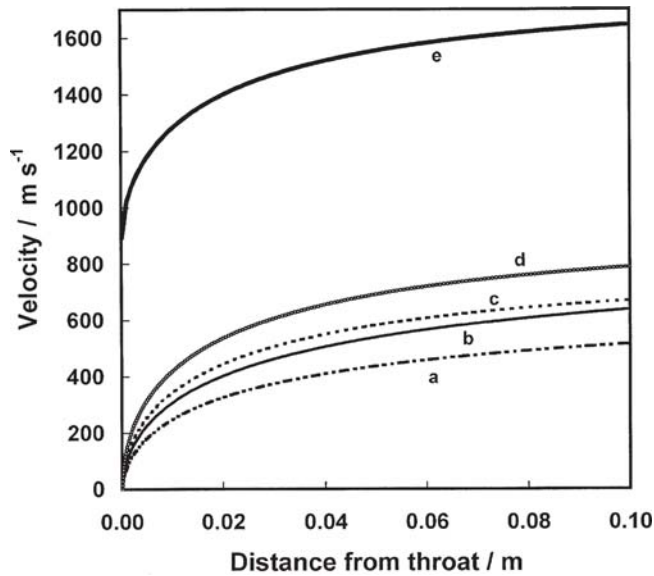
Fig. 9 Plots of velocity versus distance along the nozzle for He gas and Ti particles: (a, b) 47 and 28 μm particles, respectively, using the standard noncompressible C_d relationship; (c, d) 47 and 28 μm particles, respectively, using the compressible C_d relationship; (e) He gas at $P_0 = 29$ bar, $T_0 = 298$ K
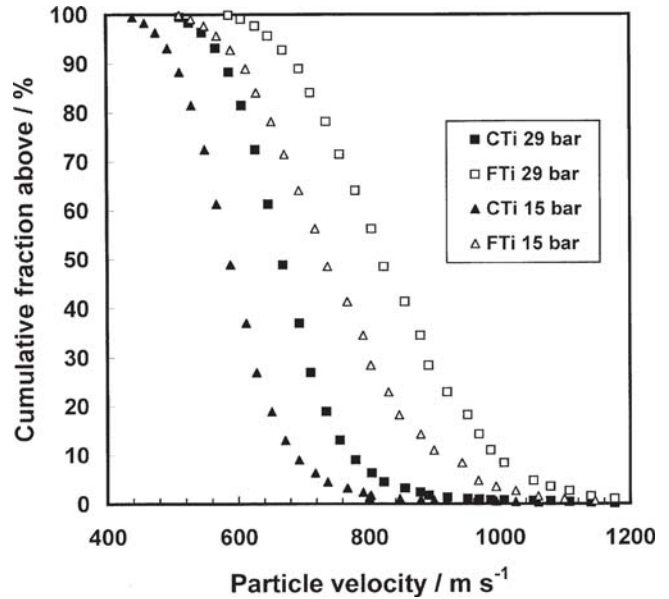

Fig. 10 Cumulative powder volume fraction velocity distributions calculated for FTi and CTi powders at gas pressures of 15 and 29 bar, as indicated in the legend; results obtained using the experimental powder size distributions shown in Fig. 2

Table 2   Thermophysical properties of materials assumed in the calculation

Property	Unit	Material	Value
Density	kg m^{-3}	Ti	4500
Specific heat capacity	J kg^{-1} K^{-1}	Ti	528
		He	5193
Thermal conductivity	W m^{-1} K^{-1}	Ti	21.6
		He	0.147
Dynamic viscosity	kg m^{-1} s^{-1}	He	1.86×10^{-5}
Specific heat ratio	…	He	1.66

$M = 4.50$. The change in gas temperature and gas velocity along the nozzle axis do not depend on stagnation pressure, provided that the nozzle is choked; thus $M = 4.50$, $V_g = 1650$ m s^{-1}, and $T_g = 39$ K for pressures of both 15 and 29 bar. However, the gas density is significantly larger at the higher stagnation pressure changing from 3.03 to 0.21 kg m^{-3} (throat to exit) at 29 bar whereas at 15 bar the change is from 1.57 to 0.11 kg m^{-3}. It is this increase in gas density at the higher stagnation pressure that is responsible for increasing particle acceleration (Eq 3) and, ultimately, the particle exit velocity. The higher stagnation pressure is also responsible for increasing the gas mass flow rate through the choked de Laval nozzle.

Calculations were performed to examine the influence of particle size on the evolution of particle velocity along the nozzle for particle diameters of 28 and 47 μm, corresponding to the mean sizes of the fine titanium (FTi) and coarse titanium (CTi) powders, respectively. Figure 9 shows particle and gas velocities at 29 bar as a function of axial position along the nozzle obtained using both the noncompressible (Eq 4) and compressible (Ref 27) drag-coefficient relationships for particle acceleration. It is seen that, irrespective of the C_d relationship used, the smaller

sized particle is initially accelerated more and reaches a higher velocity at the exit, as would be expected. It is notable that the drag coefficient relationship that is used has a very significant influence on the predicted exit velocity. This is clearly revealed by comparing curves a and c (Fig. 9) for the 47 μm particle and curves b and d (Fig. 9) for the 28 μm particle; in both cases, the exit velocity is increased by approximately 20% when compressible flow effects are included in the drag coefficient by using the Henderson equation (Ref 27). In the case of the noncompressible flow assumption (Eq 4), the Reynolds number for 28 μm particles varies from ~4000 to ~350 as the particle moves from nozzle throat to exit. This gives a change in C_d from ~0.45 to ~0.66. Similarly, C_d of the 47 μm particles changes from ~0.45 to ~0.55. However, when dependence of C_d on both M and Re is introduced, it is found that C_d typically lies in the range 0.8-1.2, which, as Eq 3 reveals, gives a significantly enhanced acceleration and, ultimately, exit velocity. Clearly, the selection of an appropriate correlation equation for the drag coefficient is an important matter to be considered if accurate numerical modeling of powder particle behavior in a cold spray nozzle is to be realized.

By calculating from the numerical model the exit velocities of particles of different sizes in the range 1-80 μm and combining this information with the experimentally determined data on powder size distribution (Fig. 2), the plots shown in Fig. 10 were produced. (The compressible drag-coefficient relationship was used to generate these plots.) These show the cumulative powder volume fraction velocity distribution for the FTi and CTi powders sprayed at 15 and 29 bar, respectively.

It is clear that the CTi powder fraction, curves a and c (Fig. 9), generally exits the nozzle at a lower velocity compared with the FTi powder, curves b and d (Fig. 9), at stagnation pressures of 15 and 29 bar. To illustrate the use of these plots consider, by way

of example, an arbitrary exit velocity of 720 m s^{-1}. It is clear that, at 29 bar pressure, ~80 vol.% of the CTi powder leaves the nozzle below this velocity, whereas only ~15% of the FTi powder particles exit below that velocity under the same conditions. Moreover, if the driving pressure is reduced to 15 bar, the fraction of powder exiting below this velocity increases to ~55% and ~95% for the FTi and CTi powders, respectively.

5. Discussion

The impact of the incoming titanium particles, in the case of both CTi and FTi powders, has evidently not caused significant deformation of the substrate close to the interface, as Fig. 4 and 5 reveal. This can be explained by considering the original microhardness of the powder (~1.7 GPa measured with 0.098 N load) and the macrohardness of the Ti6Al4V substrate material, which, in the as-received condition, is equal to ~3.0 GPa (measured with a 196 N load). This low hardness of the particles relative to the substrate will tend to localize the plastic deformation in the particle. As they deform, their plastic properties will change with work hardening (leading to an increase in hardness) and with increases in temperature due to deformation (leading to a decrease in hardness). Which of these factors will dominate is unclear; however, given that the particles are initially so much softer than the substrate indicates that plastic deformation will continue to be localized in the particle. This is illustrated in Fig. 5(c), where it is clear that the incoming particles have deformed to closely follow the rough profile of the grit-blasted substrate.

In general, porosity in cold-sprayed coatings of materials such as aluminum and copper is <1%. In contrast, the porosity in these coatings is high, irrespective of the spraying conditions, and seems to show no clear trend with increasing driving pressure. The porosity levels here are consistent with the 10-30% levels reported by Karthikeyan et al. (Ref 7), even when the deposition efficiency was >90%. These authors attributed the high coating porosity to the porosity within the sponge titanium feedstock powder that they used. In the current work, the powder particles have negligible inherent porosity, and thus the high porosity in the coating must be attributed to the lack of plastic deformation of the particles themselves on impact. This may well be associated with the hexagonal close-packed crystal structure of titanium, which exhibits very different characteristics under high rates of strain compared with copper and aluminum, which have face-centered cubic crystal structures (Ref 29).

It has been found experimentally that the deposition efficiency of the CTi powder at 29 bar is ~40%. If it is assumed that a critical velocity exists, above which a particle will deposit and below which it will simply peen the surface, then it can be deduced from Fig. 10 that the critical velocity for this powder is ~690 m s^{-1}. In this case, a deposition efficiency of ~90% would be predicted for the FTi powder under these conditions (Fig. 10), neglecting any decrease in particle velocity between nozzle exit and substrate. Such a conclusion is supported semiquantitatively by the observation (Fig. 3) that, despite the similar powder feed rates of the powders, the thickness of the coating deposited from the FTi powder is almost twice that of the coating deposited from the CTi powder (such a large difference cannot be accounted for by the 8% higher porosity observed in the coating deposited from the FTi powder). Similar high deposition efficiencies have

also been reported previously for titanium powders in cold spraying (Ref 7). Furthermore, it can be seen in Fig. 8 that the porosity in the coating deposited from the CTi powder (~14%) is somewhat less than that of the coating deposited from the FTi powder (~22%). Figure 10 indicates that a much larger proportion of the particles in the CTi powder will be traveling below the critical velocity needed for deposition than is the case for the FTi powder. It is proposed that the particles that do not deposit simply peen the coating, and the higher peening intensity for the CTi coating results in its lower porosity.

The bond-strength results (Fig. 6) show that the grit-blasted surface condition gave the lowest bond strength, with an average value around only 8 MPa, while the polished and ground surfaces resulted in significantly higher bond strengths of ~22 MPa. Although no significant increase in hardness was found by microhardness indentation (at a load of 0.98 N) below the grit-blasted surface, the grit blasting will result in the formation of a thin work-hardened zone close to the surface. Such work hardening will further limit deformation of the substrate by the incoming particles, thus hindering cold welding, which requires plastic shear deformation at the interface to disrupt surface oxides that are inevitably present. The poorer bond strength of the grit-blasted surface also implies that, in contrast to thermal spraying, the main mechanism of bonding between the substrate and the coating in cold spraying is not mechanical keying but a chemical (i.e., metallic) bond and grit blasting of the substrate surface thus appears deleterious to the promotion of good adhesion in this situation. Despite the increase in velocity at which particles exit the nozzle as the gas pressure is increased (Fig. 9 and 10) it is apparent from Fig. 7 that the bond strength of the coatings obtained by spraying FTi powder onto ground Ti6Al4V substrates depends only slightly on gas pressure. To explain this, it is proposed that the main effect of increase in pressure is not to enhance the adhesion of an individual particle whose velocity has exceeded the critical one but rather to increase the proportion of particles traveling at velocities greater than the critical velocity and thus to increase the deposition efficiency.

6. Conclusions

Titanium has been successfully cold-sprayed onto Ti6Al4V substrates. A one-dimensional model for particle movement has been developed where the effect of compressibility on the drag coefficient has been explicitly taken into account. The predicted particle exit velocity is increased by ~20% when compressible flow effects are included in the calculation of the drag coefficient. The critical velocity for deposition of this powder type is found to be approximately 690 m s^{-1}. This value is obtained by calculating the cumulative volume distribution of powder particle velocities using the numerical model and measured powder size distributions and then combining the results with estimates of deposition efficiency.

Although deposition was successful, the level of porosity is always relatively high (in the range of 13-23%) and appears to be independent of primary gas pressure. This is explained in terms of two competing effects, namely, increased particle deformation but reduced peening intensity as particle velocity increases.

The bond strength appears to be independent of gas pressure. To explain this, it is proposed that it is controlled by the weakest

link in the system, which is associated with particles depositing with a velocity near to the critical velocity. However, coatings deposited on ground substrates have higher bond strengths than those on grit-blasted substrates; it is argued that a work-hardened surface, as a result of grit-blasting, limits deformation of the substrate by impacting Ti particles and thus hinders the formation of a primary bond.

Acknowledgments

References

1. R.C. Dykhuizen and M.F. Smith, Gas Dynamic Principles of Cold spray, *J. Therm. Spray Technol.,* 1998, **7**(2), p 205-212
2. T.H. Van Steenkiste, J.R. Smith, R.E. Teets, J.J. Moleski, D.W. Gorkiewicz, R.P. Tison, D.R. Marantz, K.A. Kowalsky, W.L. Riggs II, P.H. Zajchowski, et al., Kinetic Spray Coatings, *Surf. Coat. Technol.,* 1999, **111,** p 62-71
3. A.P. Alkimov, A.N. Papyrin, and V.F. Kosarev, A Method of Cold Gas-Dynamic Deposition, *Dokl. Akad. Nauk SSSR,* 1990, **315**(5), p 1062-1065, in Russian
4. T. Stoltenhoff, H. Kreye, H.J. Richter, and H. Assadi, Optimisation of the Cold Spray Process, *Thermal Spray 2001: New Surfaces for a New Millennium,* C.C. Berndt, K.A. Khor, and E.F. Lugscheider, Ed., May 28-30, 2001 (Singapore), ASM International, 2001, p 409-416
5. C.-J. Li, W.-Y. Li, Y.-Y. Wang, and H. Fukanuma, Effect of Spray Angle on Deposition Characteristics in Cold Spraying, *Thermal Spray 2003: Advancing the Science and Applying the Technology,* B.R. Marple and C. Moreau, Ed., May 5-8, 2003 (Orlando, FL), ASM International, 2003, p 91-96
6. E. Calla, D.G. McCartney, and P.H. Shipway, Deposition of Copper by CGDS: An Investigation of Dependence of Microstructure and Properties of the Deposits on The Spraying Conditions, *Thermal Spray 2004: Advances in Technology and Application,* May 10-12, 2004 (Osaka, Japan), ASM International, 2004, p 352-357
7. J. Karthikeyan, C.M. Kay, J. Lindeman, R.S. Lima, and C.C. Berndt, Cold Spray Processing of Titanium Powder, *Thermal Spray: Surface Engineering via Applied Research,* C.C. Berndt, Ed., May 8-11, 2000 (Montréal, Québec, Canada), ASM International, 2000, p 255-262
8. D. Zhang, P.H. Shipway, and D.G. McCartney, Cold Gas Dynamic Spraying of Aluminum: the Role of Substrate Characteristics in Deposit Formation, *J. Therm. Spray Technol.,* 2005, **14**(1), p 109-116
9. D.L. Gilmore, R.C. Dykhuizen, R.A. Neiser, T.J. Roemer, and M.F. Smith, Particle Velocity and Deposition Efficiency in the Cold Spray Process, *J. Therm. Spray Technol.,* 1999, **8**(4), p 576-582
10. R.C. McCune, A.N. Papyrin, J.N. Hall, W.L. Riggs II, and P.H. Zajchowski, An Exploration of the Cold-Gas Dynamic Spray Method for Several Material Systems, *Advances in Thermal Spray Science & Technology,* C.C. Berndt and S. Sampath, Ed., Sept 11-15, 1995 (Houston, TX), ASM International, 1995, p 1-5
11. R.C. Dykhuizen, M.F. Smith, D.L. Gilmore, R.A. Neiser, X. Jiang, and S. Sampath, Impact of High Velocity Cold Spray Particles, *J. Therm. Spray Technol.,* 1999, **8**(4), p 559-564
12. K. Sakaki, N. Huruhashi, K. Tamaki, and Y. Shimizu, Effect of Nozzle Geometry on Cold Spray Process, *International Thermal Spray Conference,* E. Lugscheider and C.C. Berndt, Ed., March 4-6, 2002 (Essen, Germany), DVS Deutscher Verband für Schweißen, 2002, p 385-389
13. J. Vlcek, L. Gimeno, H. Huber, and E. Lugscheider, A Systematic Approach to Material Eligibility for the Cold Spray Process, *Thermal Spray 2003: Advancing the Science and Applying the Technology,* B.R. Marple and C. Moreau, Ed., May 5-8, 2003 (Orlando, FL), ASM International, 2003, p 37-44
14. V.F. Kosarev, S.V. Klinkov, A.P. Alkhimov, and A.N. Papyrin, On Some Aspects of Gas Dynamics of the Cold Spray, *J. Therm. Spray Technol.,* 2003, **12**(2), p 265-281
15. F. Gärtner, C. Borchers, T. Stoltenhoff, H. Kreye, and H. Assadi, Numerical and Microstructural Investigations of the Bonding Mechanisms in Cold Spraying, *Thermal Spray 2003: Advancing the Science and Applying the Technology,* B.R. Marple and C. Moreau, Ed., May 5-8, 2003 (Orlando, FL), ASM International, 2003, p 1-8
16. K. Sakaki, T. Tajima, H. Li, S. Shinkai, and Y. Shimizu, Influence of Substrate Conditions and Traverse Speed on Cold Sprayed Coatings, *Thermal Spray 2004: Advances in Technology and Application,* May 10-12, 2004 (Osaka, Japan), ASM International, 2004, p 358-362
17. A.O. Tokarev, Structure of Aluminium Powder Coatings Prepared by Cold Gas Dynamic Spraying, *Metal Sci. Heat Treatment,* 1996, **38,** p 135-139
18. J. Vlcek, H. Huber, H. Voggenreiter, A. Fischer, E. Lugscheider, H. Hallén, and G. Pache, Kinetic Powder Compaction Applying the Cold Spray Process—A Study on Parameters, *Thermal Spray 2001: New Surfaces for a New Millennium,* C.C. Berndt, K.A. Khor, and E.F. Lugscheider, Ed., May 28-30, 2001 (Singapore), ASM International, 2001, p 417-422
19. M. Grujicic, C.L. Zhao, C. Tong, W.S. DeRosset, and D. Helfritch, Analysis of the Impact Velocity of Powder Particles in the Cold-Gas Dynamic-Spray Process, *Mater. Sci. Eng.,* 2004, **A368,** p 222-230
20. K. Sakaki and Y. Shimizu, Effect of the Increase in the Entrance Convergent Section Length of the Gun Nozzle, *J. Therm. Spray Technol.,* 2001, **10**(3), p 487-496
21. T. Stoltenhoff, H. Kreye, and H.J. Richter, An Analysis of the Cold Spray Process and its Coatings, *J. Therm Spray Technol.,* 2002, **11**(4), p 542-550
22. T. Stoltenhoff, J. Voyer, and H. Kreye, Cold Spraying—State of the Art and its Applicability, *International Thermal Spray Conference,* E. Lugscheider and C.C. Berndt, Ed., March 4-6, 2002 (Essen, Germany), DVS Deutscher Verband für Schweißen, 2002, p 366-374
23. P.H. Oosthiuzen and W.E. Carscallen, *Compressible Fluid Flow,* McGraw-Hill, New York, 1997
24. R. Clift, J.R. Grace, and M.E. Weber, *Bubbles, Drops and Particles,* Academic Press, New York, 1978
25. A.B. Bailey and J. Hiatt, Sphere Drag Coefficients for a Broad Range of Mach and Reynolds Numbers, *AIAA J.,* 1972, **10,** p 1436-1440
26. M.J. Walsh, Drag Coefficient Equations for Small Particles in High-Speed Flows, *AIAA J.,* 1975, **13,** p 1526-1528
27. C.B. Henderson, Drag Coefficients of Spheres in Continuum and Rarefied Flows, *AIAA J.,* 1976, **14,** p 707-708
28. S. Trans-Cong, M. Gay, and E.E. Michaelides, Drag Coefficients of Irregularly Shaped Particles, *Powder Technol.,* 2004, **139,** p 21-32
29. W. Hubert, J.R. Meyer, and D.S. Kleponis, Modelling the High Strain Rate Behaviour of Titanium Undergoing Ballistic Impact and Penetration, *Int. J. Impact Eng.,* 2001, **26,** p 509-521